Research Article **Open Access**

S. De La Luz-Merino, M. E. Calixto*, A. Méndez-Blas, and B. Marí-Soucase

Electrodeposition and characterization of one-dimensional $CuInSe_2$ nanostructures in mesoporous silicon templates

DOI 10.1515/mesbi-2016-0009
Received October 6, 2016; revised October 20, 2016; accepted November 11, 2016

Abstract: In this work, the electrodeposition and characterization of 1D $CuInSe_2$ (CIS) nanostructures formed by the assistance of porous silicon (PSi) templates is presented. The formation of CIS was found to be potential dependent on the specific substrate being used. The filling process of the pores of PSi template was studied directly by the current transient response during electrodeposition of nanostructured CIS and results were compared with FE-SEM images. CIS nanostructures were fully characterized by using FE-SEM, FIB, XRD, and Raman spectroscopy, in order to know their physical properties.

Keywords: Inorganic compounds, Nanostructures, Semiconductors, Electrochemical techniques

1 Introduction

$CuInSe_2$ (CIS) is an important semiconductor material for thin film solar cell applications, its efficiency is dependent on its band gap value, commonly modified by the substitution of In by Ga [1]. However, it is well known that in general materials physical properties can be tuned especially when considering low dimensional systems, e.g. one-dimensional structures such as nanowires, and in the case of semiconducting materials the band gap value can be tailored by varying the diameter of the nanowires according to P. Liu et al. [2]. In fact, it is very common to use the Anodized Aluminium Oxides (AAO) template approach to grow nanowires of different materials. Several groups have used AAO templates to prepare metallic nanowires [3, 4] and nanostructured semiconductor materials such as CIS [2, 5–9], CdS [10, 11], and $Hg_{1-x}Cd_xTe$ [12]. However, there are also a few reports about using porous silicon (PSi) templates to prepare nanowires of metals [13, 14] but almost nothing on using PSi templates to grow nanowires of semiconducting materials. One of the main advantages of PSi is the availability of a wide range in pore average diameter from the microporous range <2 nm, mesoporous range from 2–50 nm and the macroporous range >50 nm, according to IUPAC. Due to this versatility, PSi offers the adequate range of pore size diameter to obtain nanostructured semiconductor materials such as CIS, where one expects that the confinement effect allows an effective increase of the band gap value in the same manner achieved for $Cu(In,Ga)Se_2$. According to the Brus Equation (1) the increment can be calculated by:

$$E = E_g + \frac{\hbar^2 \pi^2}{2r^2 \mu} \quad (1)$$

where E is the new band gap value for nanostructured semiconductor material, E_g the band gap value of bulk semiconductor, r is the nanoparticle radius in general, and μ the charge carrier reduced mass [15].

In fact, the fabrication of high-quality nanostructured CIS has been a significant research challenge and this has been basically the motivation for us to use the assistance of PSi templates. We have chosen the electrodeposition technique to obtain CIS nanowires using the template assistance and the bottom-up approach. The main advantages of ED technique are the possibility to synthesize materials inside the pores of PSi at a specific potential value which as we will see later on, depends on material and type of substrate. Moreover, the deposition process takes place at room-temperature and atmospheric pressure. ED also allows good control of deposition.

Nanostructured CIS can also be used for biomedical imaging as an alternative to Cd-based materials, opening new and interesting applications [16]. Furthermore, pre-

S. De La Luz-Merino, A. Méndez-Blas: Instituto de Física, Benemérita Universidad Autónoma de Puebla, Apartado Postal J-48, Puebla, Puebla, 72570, México
***Corresponding Author: M. E. Calixto:** Instituto de Física, Benemérita Universidad Autónoma de Puebla, Apartado Postal J-48, Puebla, Puebla, 72570, México, E-mail: ecalixto@ifuap.buap.mx
B. Marı-Soucase: IDF-Departament de Física Aplicada, Universitat Politčcnica de Valčncia, Camí de Vera s/n, 46022 Valčncia, Spain

cursor phases of copper selenides (Cu_xSe_y) leading to the formation of CIS can also be used for photothermal therapy due to its photoinduced heating when excited by NIR light at 800 nm, as was demonstrated by Hessel et al. [17].

2 Experimental

2.1 Samples preparation

The PSi layers were prepared by electrochemical etching of p-type boron-doped (100) c-Si wafers, with resistivity value of 10±3 mΩ·cm. The c-Si substrates ($\sim$1.3 cm^2) were cleaned first with ethanol and DI water using an ultrasonic bath and then submerged in a 10% HF solution to eliminate native oxides. The electrochemical etching was carried out using an electrolyte based on HF (40%) and ethanol (99.98%) in the volumetric ratio of 3:7. A power supply (Keithley model 2400) was used to deliver the current. PSi layers were obtained by applying a current density (J) of 20 mA/cm^2 over 1.0 cm^2 of exposed area (S) of the c-Si substrate. The thickness of the PSi layers can be controlled by controlling the electrochemical etching time [18]. After performing the electrochemical anodization on c-Si substrates to obtain the PSi layers, we applied high current density values during a few seconds in the electropolishing regime (J_e >600 mA) to detach the PSi layer. Then the detached PSi layer is transferred to a glass substrate coated either with a transparent conductor oxide (TCO), in this case a 500 nm SnO_2:F layer, from Pilkington Group Ltd or a sputtered 700 nm Mo layer to form the new glass/TCO or Mo/PSi template substrate [19]. The size of the active free-standing PSi layer was close to 0.5 cm^2.

ED of CIS on glass/TCO/PSi templates was carried out using an acidic aqueous buffered bath containing 2.56 mM $CuCl_2$, 9.6 mM $InCl_3$, 5.5 mM H_2SeO_3 and 1 M LiCl used as supporting electrolyte, baths were buffered using a pHydrion buffer of pH 3.00 [20]. The electrodeposition process of CIS is performed using a three-electrode ED setup system. A Pt mesh was used as the counter-electrode, a saturated calomel electrode (SCE) was used as the reference electrode; glass/TCO, c-Si wafer and glass/TCO-or-Mo/PSi template substrates were used as the working electrode. ED processes were carried out using a Voltalab model PGZ301 DYNAMIC-EIS potentiostat, at constant potential and 25 °C from a non-stirred bath. The electrochemical cell was connected to a water jacket circulator from Polyscience Ltd, with control of temperature in the range of −15 to 150 °C, which was used to ensure a constant temperature during the whole deposition process and cyclic voltammetry studies.

2.2 Materials characterization

The gravimetric method was used to calculate the porosity (P) or air fraction in PSi layers as a function of current density (J) value [18]. For the fabrication of PSi templates we performed the electrochemical anodization of c-Si under similar processing conditions at various etching times. The idea was to study how the thickness of PSi template and/or deposition conditions would affect the CIS deposition process. For that, we not only used the cyclic voltammetry (CV) technique to characterize the different substrates in an electrolytic bath containing Cu-In-Se active ionic species but also glass/TCO/PSi structures considering PSi layers of different thickness. CV measurements were carried out in Cu-In-Se baths of similar concentrations to the CIS ED baths without stirring on glass/TCO, c-Si wafer, c-Si wafer/PSi and glass/TCO/PSi template substrates. During the preliminary studies, CV scans were recorded between 0 to −2.0 V for glass/TCO and p-type c-Si substrates at a scan rate of 10 mV/s. This was done to show the potential difference between a conductive substrate (TCO) and a semiconducting substrate (c-Si). Later on, for glass/TCO and glass/TCO/PSi templates substrates, CV scans were recorded in the range of 0 to −1.0 V at a scan rate of 10 mV/s, because ultimately the ED is going to be performed on the TCO surface through the PSi template, but not over the PSi surface. In all cases, subsequent scans were recorded immediately following the initial experiments. On the other hand, electrochemical characterization of pore filling-up with CIS the PSi template was carried out by current transient analysis recorded during deposition.

A field emission scanning electron microscopy (FE-SEM) attached to an energy dispersive X-ray spectroscopy (EDS) analytical system was used as the primary tool to characterize first the PSi template, and the new formed glass/TCO/PSi template substrates. FE-SEM also was used to study the surface morphology of the glass/TCO/PSi template/CIS structures and to get information on the infiltration of CIS into the pores we used Focus Ion Beam (FIB). X-ray diffraction studies were performed on glass/Mo/PSi template/CIS in the BB mode, using a Rigaku Ultima-IV system with a Cu Ka (A = 1.54 Å) radiation. Raman studies were also performed using a Horiba Jobin Yvon (HR) LabRaman Spectrometer equipped with a microscope and a 10 mW He-Ne laser with an emission line of 632 nm.

3 Results and Discussion

In this work, 2.5 µm-PSi layers of ∼70% porosity and 20 nm pore size diameter fulfilled the pore diameter, conductivity and mechanical strength requirements to be used as PSi templates. Figure 1 shows a FE-SEM image of a freshly prepared PSi layer with an average pore size diameter ∼20 nm. The above mentioned conditions were established after optimization of anodization parameters. PSi layers of different thicknesses (from 10–1 µm) were prepared and peeled-off from the c-Si wafer, and transferred to the glass/TCO substrate [19].

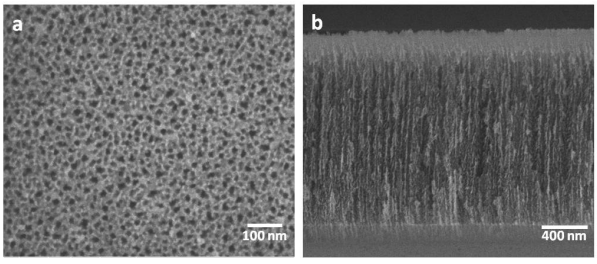

Figure 1: (a) FE-SEM image of freshly prepared 2.5 µm-PSi layer of ∼70 porosity, and pores with an average size diameter ∼20 nm. (b) Cross section view.

However when performing the CV to the glass/TCO/PSi templates (of 10 and 5 µm) we realized that the voltammograms did not resemble the ones performed on glass/TCO or c-Si wafer, besides the highest current registered was very low (−0.15 mA). After analyzing those prepared samples we found out that they were composed mainly of Cu_xSe_y, which means that the deposition mechanism was different and no $CuInSe_2$ was formed. However for 2.5 and 1 µm PSi layers the voltammograms were somehow very similar to that performed on glass/TCO. For the case of c-Si wafers, voltammograms showed a shifting towards higher negative potentials but basically they preserve most of the features of that performed on glass/TCO, which was expected due to the different electrode potential between a metal and a semiconducting substrate.

Incidentally, it is important to mention that 2.5 µm PSi layers kept their mechanical strength and morphology, even after being detached from the c-Si wafer substrate and being transferred to the glass/TCO substrate, when compared to the 1 µm PSi layer.

CV data give information about the reaction mechanism and formation of CIS on the substrates used; CV studies were performed on glass/TCO and c-Si wafer substrates first to figure out the potential range values for the deposition of CIS on each type of substrate. The reason of using glass/TCO substrates was because we wanted to have direct comparison of glass/TCO and glass/TCO/PSi template substrates and because ultimately the electrodeposition of CIS was going to take place at the surface of the TCO through the pores of PSi template and hopefully not over the PSi template.

CV studies were performed from a bath containing Cu-In-Se ionic species, similar to that used for the electrodeposition of CIS, without stirring at 25 °C. Figure 2 shows the first two scans of the Cu-In-Se of the aqueous buffered baths performed on (a) glass/TCO, (b) c-Si wafer and (c) glass/TCO/2.5 µm-PSi template substrates. The appearance of peaks in the CV indicates a redox reaction as occurring at the electrode, either in solution or on the surface; the sharpness of peaks, indicates that the redox reactions are mostly related to the electrode surface.

Figure 2(a) shows a very slow current increase in the 0 to −0.3 V potential ranges where the formation of Cu_xSe_y phases and possible the formation of elemental Se occurs according to equations (2-8) [5, 21]. Then at −0.4 V there is a fast current increase in the negative direction showing the formation of a very well defined and strong peak (peak A), indicating the reduction process of Cu_3Se_2 to $Cu_{2-x}Se$ phases and the incorporation of In [5, 21]:

$$Cu^{2+} + Se + 2e^- \leftrightarrow CuSe \tag{2}$$

$$2CuSe + 2e^- \rightarrow Cu_2Se + Se^{2-} \tag{3}$$

$$2Cu^{2+} + SeO_3^{2-} + 6H^+ + 8e^- \rightarrow Cu_2Se + 3H_2O \tag{4}$$

$$2Cu^{2+} + 4e^- + Se \leftrightarrow Cu_2Se \tag{5}$$

$$Cu_2Se + 2H^+ + 2e^- \leftrightarrow 2Cu(s) + H_2Se \tag{6}$$

$$3Cu^{2+} + 2Se + 6e^- \leftrightarrow Cu_3Se_2 \tag{7}$$

$$H_2SeO_3 + 4H^+ + 4e^- \leftrightarrow Se + 3H_2O \tag{8}$$

Besides, Cu_3Se_2 is known to be the first stage reduction process that leads to the formation and growth of $CuInSe_2$ and with the incorporation of In starting at −0.4 V in the form of In_2Se_3 according to equations (9-12), at higher potentials more In is incorporated, leading to the formation of In rich $CuInSe_2$ at ∼ −0.7 V.

$$In^{3+} + 3e^- \leftrightarrow In \tag{9}$$

$$2In^{3+} + 3Se + 6e^- \leftrightarrow In_2Se_3 \tag{10}$$

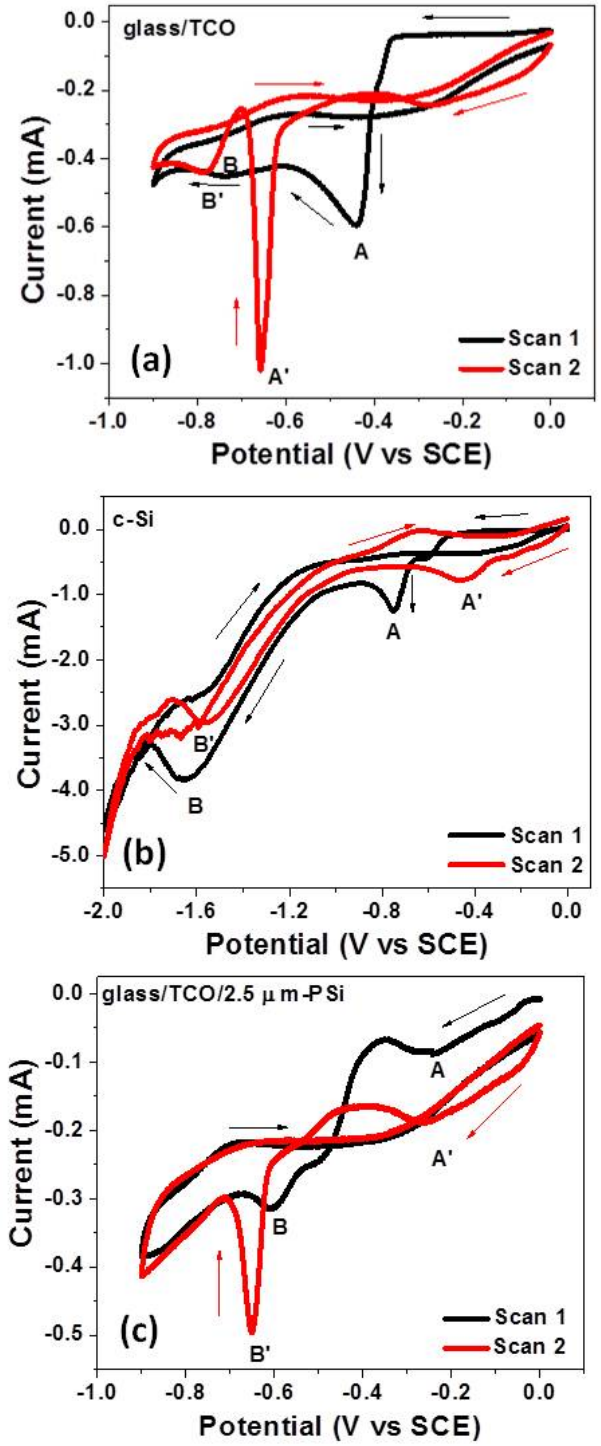

Figure 2: CV plots for first two scans of an aqueous Cu-In-Se buffered bath on (a) glass/TCO, (b) c-Si and (c) glass/TCO/2.5 µm-PSi template substrates.

$$Se^{2-} + 2H^{+} \leftrightarrow H_2Se \tag{11}$$

$$3H_2Se + 2In^{3+} \leftrightarrow In_2Se_3 + 6H^{+} \tag{12}$$

In the second scan, and all subsequent scans, at lower potential a small hump centred at −0.2 V is observed, but peak A has disappeared, this observation is in agreement to the effect observed by M.C.F. Oliveira et al. [22] This effect is directly related to the electrode surface. Besides, from an electrolytic bath at pH of ∼2.5, H_2Se is very likely the phase to be formed from dissolved Se^{2-} [23]. The generated H_2Se will react with In^{3+} forming more In_2Se, which will react immediately with Cu_2Se to form the $CuInSe_2$ film according to equation (13) [5, 21]:

$$Cu_2Se + In_2Se_3 \leftrightarrow 2CuInSe_2 \tag{13}$$

The whole electrode reaction has been described as a multistep process [22, 24], and the overall reaction can be written according to equation (14):

$$Cu^{2+} + In^{3+} + 2H_2SeO_3 + 8H^{+} + 13e^{-} \rightarrow CuInSe_2 + 6H_2O \tag{14}$$

In the second and all subsequent scans of Figure 2a, peak B, now B' shifts towards more negative potential values. It is very likely that copper selenides are no longer formed at the same rate on the modified surface of the glass/TCO and that the formation of In_2Se_3 and $CuInSe_2$ phases are more favoured at higher potentials. In fact, it has been found that Cu-In-Se can be obtained when the deposition potential is set between −0.4 and −0.7 V, but the growth of CIS with very close chemical composition to the stoichiometry of $CuInSe_2$ can be formed when using a potential between −0.5 to −0.55 V [25]. The rise in current at −0.9 V is due to the beginning of the hydrogen evolution/solvent reduction reaction.

As was previously described, PSi is going to be used only as a template to perform the ED of CIS. Because of this, it was necessary to ensure first that the role of PSi template was only to act as a guide for the active ionic species of Cu^{2+}, In^{3+} and Se^{4+} to be reduced at the glass/TCO surface allowing them to pass all the way through the PSi template thickness. In order to verify such hypothesis, same CV studies were performed on c-Si substrates. Figure 2b shows the CV of a c-Si wafer substrate in a similar bath as in Figure 1a. Figure 2b shows a very slow current increase in the 0 to −0.4 V potential ranges. In a similar way as in Figure 2a, in this potential range the formation of copper selenide phases is expected. At −0.6 V a very small hump can be clearly observed which might be related to the reduction of elemental Se and CuSe, then an increase of current in the negative direction is observed forming a small peak centred at −0.8 V, the appearance of such peak, identified as peak A, indicates also the reduction process of Cu_3Se_2 to $Cu_{2-x}Se$ phases and the initial intake of In^{3+} [22].

In the second scan, and all subsequent scans, at lower potential a small hump centred at −0.4 V is observed, now identified as peak A', but peak A has disappeared, in a similar way as in Figure 2a. The incorporation of indium into the growing film occurs via chemical reaction with H_2Se to form In_2Se_3, which is rapidly assimilated into the growing film by reaction with Cu_3Se_2 to form $CuInSe_2$. Another reduction peak at $\sim$ −1.6 V, peak B, is also observed in the first scan of Figure 2b, this peak might be related to the formation of $CuInSe_2$ besides an excess of elemental Se. However, in the second and all subsequent scans, peak B, now B', shift towards less negative potential values. It is very likely that copper selenides are no longer formed at the same rate on the modified surface of the c-Si and that the formation of In_2Se_3 and $CuInSe_2$ phases are more favoured at higher potentials. Finally, a current increase is observed which starts at −1.8 V due to the beginning of the hydrogen evolution/solvent reduction reaction. In a similar way, CV scanning was performed on glass/TCO/2.5 µm-PSi template substrates in a bath similar to the above. Figure 2c shows a current increase in the potential range from 0 to −0.25 V in the first scan, and once again similar to the previous cases at lower potential values occur the formation of CuSe and possibly an excess of Se. At −0.25 V the formation of a small peak, peak A, is observed. It is evident that when comparing this first cyclic voltammogram with the previous ones of the other systems, it is quite different, which reveals that the electrode reactions occurring on the new glass/TCO/PSi substrate are not the same to those of the glass/TCO or even the c-Si wafer substrates. This effect is due to the glass/TCO modified surface where the PSi layer is superimposed over the top of the substrate. At −0.5 V a small shoulder is formed which might be related to the formation of elemental Se, and then there is a current increase forming a small peak, peak B, centred at −0.6 V, which is related to the intake of In^{3+}, that reacts with H_2Se forming thus In_2Se_3 which transforms then to $CuInSe_2$ by the reaction with Cu_3Se_2. At −0.9 V a current increase is observed, which indicates the beginning of the hydrogen evolution/solvent reduction reaction. In the second and all subsequent scans, a similar behavior is observed as shown in Figure 2a, first a current increase and then the formation of a small peak, peak A', very close to the same potential value as in the first scan $\sim$ −0.25 V, indicating the formation of copper selenide phases, then an almost lineal current increase in the −0.45 to −0.6 V range, that ends with the formation of a very large peak, identified as peak B'. The sharpness of peak B' indicates that the electrochemical process is related to the electrode surface, i.e. the formation of nanostructured $CuInSe_2$ into the PSi template substrate. At even higher potential a current increase is observed, indicating the hydrogen evolution/solvent reduction reaction.

Comparing CV results of the aqueous Cu-In-Se electrolyte system on glass/TCO and c-Si wafer substrates, we would expect the growth of Cu-In-Se with a chemical composition very close to the stoichiometric $CuInSe_2$ at $\sim$ −0.5 V and at $\sim$ −1.2 V vs. SCE, respectively. So, that the hypothesis we propose was that by doing the ED at −0.5 V on glass/TCO/2.5 µm-PSi template substrates the formation and growth of CIS would be on the glass/TCO substrate surface, not onto c-Si or PSi. However, by comparing Figure 2c with Figures 2a and 2b, it becomes clear that the current values are rather low; this might be explained if we recall that the PSi template is expected to act as a physical barrier and chemically inert superimposed pattern on the glass/TCO surface, which is believed to be slowing down the formation of copper selenides and the intake of In^{3+} for the formation of In_2Se_3 which eventually will transform to $CuInSe_2$ by the reaction with Cu_3Se_2.

Moreover, most of the pores go through the whole thickness of the PSi template and contain branches of smaller size than the pore diameter, according to studies performed by Zhang et al. [26]. Such an effect can be observed in Figure 1b. So, limitations in mass transfer may arise in some pores because the path of the ions can be very tortuous in their way to reach the TCO surface throughout the PSi template thickness [27–29]. In order to compensate the low current effect, we decided to increase the deposition potential, so that instead of using −0.5 V we performed the deposition of CIS at −0.7 V on glass/TCO/2.5 µm-PSi template substrates. We deposited first a CIS film on glass/TCO substrates at the above mentioned potential to promote the incorporation of more In to the film, EDS results showed that at such potential we can obtain a film with the following composition: 23.49 at % Cu, 27.87 at% In and 48.65 at % Se. In a similar way, we expect to favour the formation of nanowires of CIS inside the PSi template.

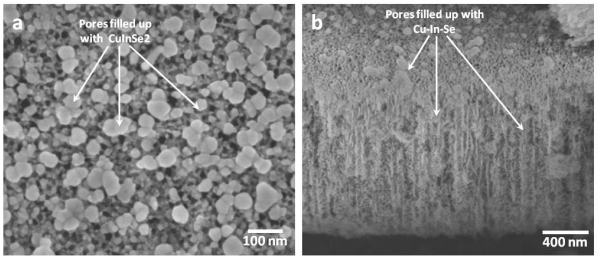

Figure 3: FE-SEM image of the electrodeposition of CIS at −0.7 V vs. SCE during 3 min. on glass/TCO/2.5 µm-PSi template substrate (a) front view and (b) cross section view.

The deposition time was set to 3 min, because if the deposition is allowed to be longer, the filling up process of the pores would take place first and then they would overflow, giving the formation of caps on top of the PSi template surface until finally starting the growth of a continuous CIS layer. Figure 3 shows the FE-SEM results of the electrodeposition of CIS into the glass/TCO/2.5 µm-PSi template substrate performed during 3 min at −0.7 V. A chemical composition analysis of this sample was performed and it was found that the CIS growth inside the pores of PSi template consisted of 20.36 at% Cu, 18.84 at% In and 60.81 at% Se, as we reported previously [19]. According to the EDS results the 1D CIS nanostructures have a Cu/In ratio = 1.08 and a fairly large amount of selenium.

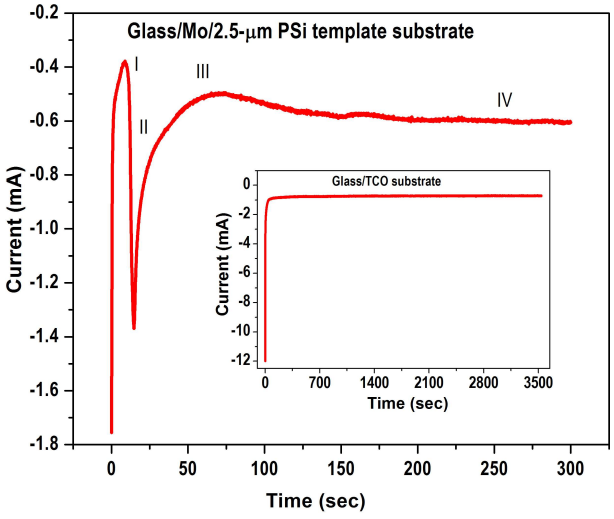

Figure 4: Transient current response for the electrodeposition of nanostructured CIS on a glass/Mo/2.5 µm-PSi template substrate and for a CIS thin film on glass/TCO substrate (inset).

Besides, during the electrodeposition process of nanostructured CIS within the pores of the glass/Mo/2.5 µm-PSi template substrate, we recorded the typical chronoamperometry response; current vs. time, see Figure 4. According to this figure, four different zones can be clearly identified in the same way as Molares et al. [30]: a sharp current increase (I), related to the nucleation stage, growth of CIS nanowires inside pores with an average diameter of 20 nm of the PSi template substrates (II), pores already filled-up and caps starting to form on the top (III) and finally a continuous and homogeneous CIS layer starts to form on top of the surface of the glass/TCO/2.5 µm-PSi template substrate (IV). This last process is very characteristic in a transient current response during the growth of a CIS layer at a constant potential. Inset of Figure 4 shows the chronoamperometry graph during the electrodeposition process of a CIS thin film on a glass/TCO substrate at −0.7 V vs. SCE. Such behaviour helped us to establish the electrodeposition time needed to fill up the pores and to avoid the growth of the CIS layer on top of the PSi template substrate, which was corroborated afterwards by FE-SEM images. In our case, we found out that 3 min deposition was enough to grow and form nanostructured CIS inside the pores of PSi template substrates.

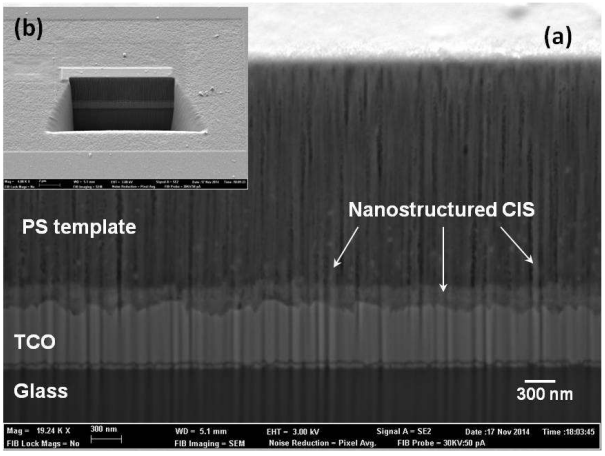

Figure 5: (a) FIB/SEM cross-section images of the glass/TCO/2.5 µm-PSi template/1D CIS nanostructures obtained by ED and (b) a FIB/SEM milling image of sample using gallium ions.

In order to know more about the filling process of the PSi template with CIS we use a FIB/SEM combination system to mill and cross-section imaging a small section of the glass/TCO/2.5 µm-PSi template infiltrated with CIS. FIB/SEM imaging results are shown in Figure 5. From these images we can observe that the ED of 1D CIS nanostructures has taken place, being able to grow nanowires of ∼300 nm along the pores of PSi template. This Figure also shows the formation of irregular growth of CIS particles along the pores of PSi template.

On the other hand, according to EDS results, ED nanostructured $CuInSe_2$ has excess selenium, so that in order to determine the source of that extra selenium present, we performed a qualitative Raman spectroscopy. Figure 6a shows Raman results for c-Si/p-Si, according to this graph we can observe a very intense and narrow peak located at 518 cm^{-1} which corresponds to the phononic mode of PSi, which is shifted from that of c-Si located at 520 cm^{-1} [31]. Raman results are also shown for a typical ED CIS thin film, in this case two peaks can be easily identified, a very large and narrow peak located at 173 cm^{-1} which corresponds to the characteristic A_1 vibrational mode of the CIS thin

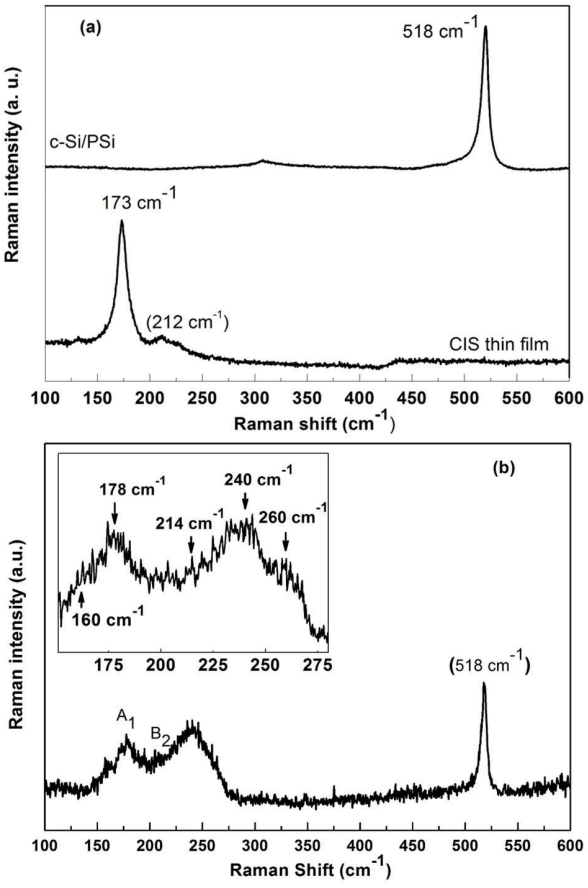

Figure 6: Raman spectroscopy of (a) c-Si/PSi and as-deposited CIS thin film and (b) of nanostructured CIS formed on glass/TCO/2.5 µm-PSi template substrates.

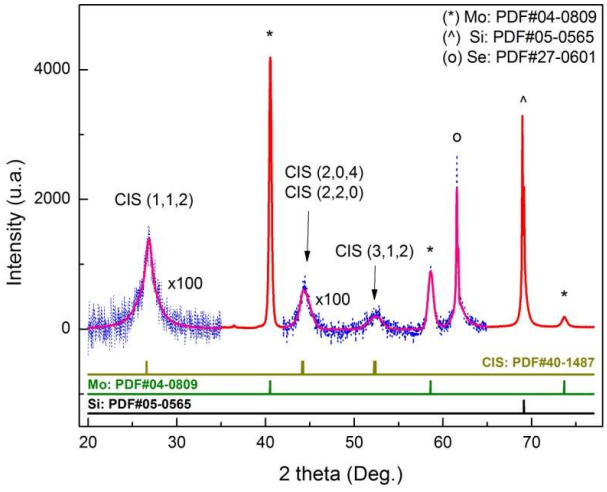

Figure 7: XRD pattern of nanostructured CIS on glass/Mo/2.5 µm-PSi template substrate electrodeposited at −0.7 V vs. SCE for 3 minutes.

film. The second is a very small and broad peak located at ~212 cm^{-1} corresponds to the B_2 mode of $CuInSe_2$ phase according to [32].

Figure 6b, shows three intense peaks clearly observed, the largest and very narrow Raman peak located at 518 cm^{-1} corresponds to the phononic mode of PSi template. The other two intense and broad Raman peaks are located in the range of 100–300 cm^{-1}, the first peak is located at 178 cm^{-1} and the second one at 240 cm^{-1}, but on both peaks there are shoulders located at 160 cm^{-1} and 260 cm^{-1} (see inset of Fig. 6b). The peak centred at 178 cm^{-1} corresponds to the characteristic A_1 vibrational mode of the chalcopyrite $CuInSe_2$ nanostructured phase, as reported by Izquierdo-Roca et al. [33] while the shoulder at 160 cm^{-1} has been associated to the $CuIn_2Se_{3.5}$ phase, above than the reported value of 156 cm^{-1} [34, 35]. The peak centred at 240 cm^{-1} is attributed to the presence of elemental trigonal Se [33, 36] while the contribution of shoulder at 260 cm^{-1} is attributed to Cu_xSe_y compounds [32, 36–38].

The formation of nanostructured $CuInSe_2$ inside the pores of the PSi template was studied also by XRD. Figure 7 shows the XRD results for the electrodeposition of one-dimensional CIS growth into the pores of PSi template substrates. According to this graph, three main peaks can be observed at 26.80°, 44.42° and 52.39°, respectively, which correspond to the diffraction pattern of CIS at (112), (220/204) and (312) polycrystalline reflections (PDF 40-1487). XRD measurements from nanostructured CIS had to be performed separately for each individual peak by using the appropriated setting values in the XRD equipment. For that, the peaks associated to (112) and (220/204) and (312) planes, had to be increased by a factor of 100, in order to represent them in the same XRD graph with the peaks corresponding to Si from the PSi template and Mo from the glass/Mo substrate. The reason for doing this, was that the intensity of the diffraction patterns of Si and Mo was very high compared to that of nanostructured CIS.

Also a large peak located at 61.56° can be observed which could correspond either to that of elemental Se with hexagonal structure (PDF 27-0601) or to the $Cu_{2-X}Se$ (PDF 47-1448), both considered as secondary phases detected by Raman spectroscopy. XRD measurements in the BB mode were performed on glass/Mo/2.5 µm-PSi template instead on glass/TCO/2.5 µm-PSi template substrates, because the main peak (112) of CIS is located at the same main peak position of TCO (SnO_2:F). It is important to clarify that it was not possible to perform GIXRD measurements on these samples even by modifying and adjusting the setting of the XRD equipment to selected incident angles such as 0.2, 0.3 or even 0.5 deg, because the only response detected was that of Si from the PSi template. By doing this experi-

ment we have confirmed that the obtained XRD spectrum corresponds to the infiltration of CIS into the PSi template, i.e. to the CIS nanowires not to the CIS deposited on top of the PSi template surface.

As part of the optical characterization, we have made a rough estimation of the band gap value of the electrodeposited nanostructured CIS using Tauc equation by plotting $h\nu$ vs $(\alpha h\nu)^2$, taking into account the linear behavior near the absorption edge and extrapolating with a straight line when $(\alpha h\nu)^2 = 0$ and $E_g = h\nu$ [39]. The absorption coefficient (α) was calculated from transmittance measurements (T) by using equation (15) [40]:

$$\alpha = \frac{1}{d}\ln\left[\frac{(1-R)^2}{2T} + \left[\frac{(1-R)^4}{4T^2} + R^2\right]^{\frac{1}{2}}\right] \qquad (15)$$

where d is the thickness of the CIS layer and $R = [(n-1)/(n+1)]^2$, considering the air as one of the media. In our case, according to FIB/SEM images (Figure 5), the length of the ID CIS nanostructures is ~300 nm but the pores of PSi template are not filled, and moreover they contain also CIS nanoparticles which can be observed along the thickness of PSi template. So that we have considered an effective media and we propose some different values for thickness $d = d_e$. In all the measurements we used an empty glass/TCO/PSi template substrate as our reference in order to record just the nanostructured CIS optical response.

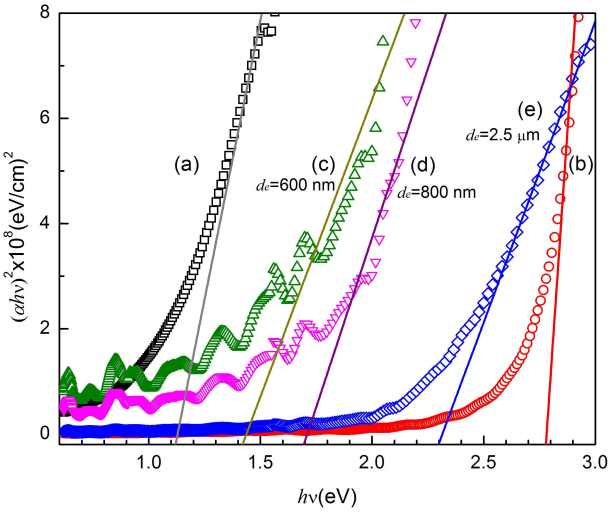

Figure 8: Estimation of the band gap value for (a) as-deposited CIS thin film, (b) glass/TCO/PSi template substrate and (c-e) glass/Mo/2.5 μm-PSi template/CIS considering different d_e values

The calculated band gap value was estimated from the $h\nu$ vs $(\alpha h\nu)^2$ plotting for different d_e values as shown in Figure 8. If d_e = 2.5 μm, same thickness of PSi template, it would mean that pores are completely filled with CIS. Under such conditions the estimation of band gap value would be 2.33 eV. However, according to Omata et al. [41], the CIS band gap value is expected to increases rapidly from 1.5 to 3.2 eV, as the diameter of nanoparticles decreases from 6 to 1 nm. Therefore, it is reasonable not to expect a drastic change in the band gap value because the average pore diameter value is ~20 nm; a 2.33 eV band gap value for nanostructured CIS would not be consistent with the results.

Also, when considering a partial CIS filling, i.e. 25%–30% of the total PSi template thickness, d_e would be close to 600–800 nm, so under these conditions the calculated band gap would be in the range of 1.39–1.7 eV. However, according to FIB/SEM images (Figure 5), the thickness of the one-dimensional CIS nanostructures is ~300 nm, so the band gap would be in the range of 1.10–1.29 eV, where the lowest value (~1.10 eV) corresponds to an as-deposited CIS thin film. This increase can only be attributed to the nanometric size effects of CIS confined by the pores of the PSi template [42]. On the other hand, Figure 8 also shows the band gap value (2.78 eV) of an empty glass/TCO/PSi template.

The influence of secondary phases such as $Cu_{2-x}Se$ (E_g ~ 2.21–2.39 eV) and elemental Se (E_g = 1.6 eV) formed during electrodeposition on the band gap value of one-dimesional CIS nanostructures, must be avoided. In such case, the bottom-up method to grow one-dimensional CIS nanostructures by electrodeposition would prove to be a reliable way to grow this type of nanostructured materials.

4 Conclusions

While the ED of CIS thin film on glass/TCO (Mo) substrates can be straightforward, its confinement into PSi templates opens the possibility of band gap tuning. It was demonstrated that nanostructured CIS can be formed by ED into pores of 20 nm average size diameter and 2.5 μm-PSi template substrates by applying a potential value of −0.7 V vs. SCE during 3 min, using an aqueous buffered bath. The minimum in the current transient curve and FIB/SEM images confirm the partial filling process of pores. The formation of nanostructured CIS was also confirmed by XRD studies. FIB/SEM images showed that the thickness of the one-dimensional CIS nanostructures is ~300 nm; for such a value it would correspond to a band gap in the range of 1.10–1.29 eV. Such an increase could be attributed to the nanometric size effects of CIS confined by the pores of

the PSi template. Additionally, it was demonstrated that it is possible to obtain by ED, nanostructured secondary phases based on Cu_xSe_y, which have recently being reported as biocompatible photothermal material for cancer therapy.

Acknowledgement: This work was partially supported by BUAP/PROFOCIE funds provided through the CA: Física Aplicada, CONACYT under the project Grant No. 167993, CEMIE-Sol P26 and IRSES Marie Curie People FP7 grant 269279. All the authors contributed equally to this work.

References

[1] P. Jackson, D. Hariskos, E. Lotter, S. Paetel, R. Wuerz, R. Menner, W. Wischmann, and M. Powalla, *Prog. Photovolt: Res. Appl.*, 19 (2011) 894.

[2] P. Liu, V. P. Singh, S. Rajaputra, S. Phok, Z. Chen, *J. Mater. Res.* 25 (2010) 207.

[3] H. J. Wang, C. W. Zou, B. Yang, H.B Lu, C.X. Tian, H.J. Yang, M. Li, C.S. Liu, D.J. Fu, J.R. Liu, *Electrochem. Communications* 11 (2009) 2019.

[4] J. M. Baik, M. Schierhorn, M. Moskovits, *J. Phys. Chem. C,* 112 (7) (2008) 2252.

[5] Pin-Kun Hung, Tsung-Hau Lin and Mau-Phon, *J. Electrochem. Soc.* 161(3) 2014 D79-D86.

[6] E. A. Hernández-Pagán, W. Wang, and T. E. Mallouk, *ACS Nano* 5 (2011) 3237.

[7] M. K. Date, B. C. Chiu, C. H. Liu, Y. Z. Chen, Y. C. Wang, H. Y. Tuan, Y. L. Chueh, *Mater.Chem. Phys*. 138, 1 (2013) 5.

[8] M. Pashchanka, J. Bang, N. S. A. Gora, I. Balog, R. C. Hoffmann, J. J. Schneider *Beilstein J. Nanotechnol.* 4 (2013) 868.

[9] D. T. Schoen, H. Peng, Y. Cui, *ACS Nano* 7(2013) 3205.

[10] S. Poduri, M. Dutta, M. Stroscio, *J. of Elec. Materials*, 43, 11 (2014) 3979.

[11] A. Aguilera, Vivekanand Jayaraman, S. Sanagapalli, R. S. Singh, Visweswaran Jayaraman, K. Sampson, V. P. Singh, *Solar Energy Materials & Solar Cells* 90 (2006) 713.

[12] B. A. Ashenfelter, T. P. Bigioni, *Materials Science in Semiconductor Processing*, 25 (2014) 18.

[13] S. Aravamudhan, K. Luongo, P. Poddar, H. Srikanth, S. Bhansali, *Appl. Phys. A* 87, (2007) 773.

[14] K. Fukami, Y. Tanaka, M. L. Chourou, T. Sakka, Y. H. Ogata, *Electrochimica Acta* 54 (2009) 2197.

[15] L. E. Brus, *J. Chem. Phys.* **80** (1984) 4403

[16] E. Cassette, T. Pons, C. Bouet, M. Helle, L. Bezdetnaya, F. Marchal, B. Dubertret, *Chem. Mater.* **22** (2010) 6117.

[17] C. M. Hessel, V. P. Pattani, M. Rasch, M. G. Panthani, B. Koo, J. W. Tunnell, and B. A. Korgel, *Nano Lett.* **11** (2011) 2560

[18] S. De La Luz Merino, F. Morales-Morales, A. Méndez-Blas, M. E. Calixto, F. G. Nieto-Caballero, G. García-Salgado, *Appl. Phys. A: Mater. Sci. Process.* 111 (2013) 1077.

[19] S. De La Luz-Merino, Ma. Estela Calixto, A. Méndez-Blas, *Materials Chemistry and Physics,* 163 (2015) 362.

[20] M. E. Calixto, K. D. Dobson, B. E, McCandless, R. W. Birkmire, in *Conf. Rec. 31st IEEE Photovoltaic Spec. Conf*. 2005, p. 378.

[21] L. Kaupmees, M. Altosaar, O. Volubujeva, E. Mellikov, *Thin Solid Films* 515 (2007) 5891

[22] M.C.F. Oliveira, M. Azevedo, A. Cunha, *Thin Solid Films*, 405 (2002) 129.

[23] M. Estela Calixto, Kevin D. Dobson, Brian E. McCandless, and Robert W. Birkmire, *J. Electrochem. Soc.*, 153, 6 (2006) G521.

[24] E. Chassaing, O. Ramdani, P.P. Grand, J.F. Guillemoles, D. Lincot, *Phys. Stat. Sol. (c)* 5 (2008) 3445.

[25] M. E. Calixto, K. D. Dobson, B. E. McCandless and R. W. Birkmire, *Mater. Res. Soc. Symp. Proc.* 2005, 865, F14.17.1.

[26] X. G. Zhang, *J. Electrochem. Soc.*, 151 (1) (2004) C69

[27] F.A. Harraz, S.M. El-Sheikh, T. Sakka, Y.H. Ogata, *Electrochim. Acta*, 53 (2008) 6444.

[28] F. A. Harraz, *Appl. Surf. Sci.* 287 (2013) 203.

[29] S. Aravamudhan, K. Luongo, P. Poddar, H. Srikanth, S. Bhansali, *Appl. Phys. A: Mater. Sci. Process.,* 87 (2007) 773.

[30] M. E. Toimil Molares, J. Brotz, V. Buschmann, D. Dobrev, R. Neumann, R. Scholz, I.U. SchuchertC. Trautmann, J. Vetter, *Nuclear Instruments and Methods in Physics Research B* 185 (2001) 192.

[31] C.H. Cho, Y.S. Seo, H. Na, Y. Kim, *J. Korean Phys. Soc*. 33 (1998) 292.

[32] C. Rincón, F. J. Ramlrez, *J. Appl. Phys.* 72 , 9 (1992) 4321.

[33] V. Izquierdo-Roca, J.A. lvarez-García, b L. Calvo-Barrio, A. Perez-Rodríguez, J.R. Morante, V. Bermudez, O. Ramdani, P.-P. Grand, O. Kerrec, *Surf. Interface Anal*. 40 (2008) 798.

[34] C.M. Xu, X.L. Xu, J. Xu, X.J. Yang, J. Zuo, N. Kong, W.H. Huang, H.T. Liu, *Semicond. Sci. Technol*. 19 (2004) 1201.

[35] V.V. Poborchii, A.V. Kolobov, K. Tanaka, *Appl. Phys. Lett.* 72 (1998) 1167.

[36] O. Ramdani, J.F. Guillemoles, D. Lincot, P.P. Grand, E. Chassaing, O. Kerrec, E. Rzepka, *Thin Solid Films* 515 (2007) 5909.

[37] M. Ishii, K. Shibata, H.J. Nozaki, *Solid State Chem*. 105 (1993) 504.

[38] B. Minceva-Sukarova, M. Najdoski, I. Grozdanov, C.J. Chunnilall, *J. Mol. Struct.* 410 (1997) 267.

[39] J. Tauc, *Material Research Bulletin*, 3, 1 (1968) 37

[40] J. Gonzalez-Hernandez, P.M. Gorley, P.P. Holrley, O.M. Vartsabyuk, Yu.V. Vorobiev, *Thin Solid Films*, 403–404 (2002) 471

[41] T. Omata, K. Nose, S. Otsuka-Yao-Matsuo, *J. Appl. Phys.*, 105 (2009) 073106

[42] L. Shi, C. Pei, Q. Li, *Nanoscale*, 2 (2010) 2126